IEICE TRANS. FUNDAMENTALS, VOL.E105–A, NO.3 MARCH 2022

PAPER

A Sparsely-Connected OTFS-BFDM System Using Message-Passing Decoding

Tingyao WU[†a)], **Zhisong BIE**[†b)], ***Nonmembers***, ***and*** **Celimuge WU**[††c)], ***Member***

SUMMARY The newly proposed orthogonal time frequency space (OTFS) system exhibits excellent error performance on high-Doppler fading channels. However, the rectangular prototype window function (PWF) inherent in OTFS leads to high out-of-band emission (OOBE), which reduces the spectral efficiency in multi-user scenarios. To this end, this paper presents an OTFS system based on bi-orthogonal frequency division multiplexing (OTFS-BFDM) modulation. In OTFS-BFDM systems, PWFs with bi-orthogonal properties can be optimized to provide lower OOBE than OTFS, which is a special case with rectangular PWF. We further derive that the OTFS-BFDM system is sparsely-connected so that the low-complexity message passing (MP) decoding algorithm can be adopted. Moreover, the power spectral density, peak to average power ratio (PAPR) and bit error rate (BER) of the OTFS-BFDM system with different PWFs are compared. Simulation results show that: i) the use of BFDM modulation significantly inhibits the OOBE of OTFS system; ii) the better the frequency-domain localization of PWFs, the smaller the BER and PAPR of OTFS-BFDM system.

key words: *orthogonal time frequency space, bi-orthogonal frequency division multiplexing, out-of-band emission, peak-to-average ratio, bit error rate*

1. Introduction

Orthogonal time frequency space (OTFS) has been recently proposed to satisfy the scenes of high Doppler or high carrier frequencies in next-generation mobile communications (5G and above), such as high-speed trains, vehicle-to-vehicle, millimeter-wave communications [1]–[5]. The key idea of OTFS is to transform the information signal from the delay-Doppler (DD) domain to the time-frequency (TF) domain by adding the two-dimensional (2D) inverse symplectic finite Fourier transform (ISFFT) on top of the orthogonal frequency division multiplexing (OFDM) modulation. As a result, the information carried on each transmission symbol is evenly distributed over all TF lattice points on a given frame. Combined with proper equalization, OTFS can extract the full channel diversity over time and frequency, which means the channel gain of each symbol in the data frame is almost constant. Other attractive features are: i) a conceptual connection between Radar and communications [6], [7]; ii) the possibility of combining ISFFT transform with various multi-carrier modulations (not limited to OFDM) [8]; iii) the sparse-connectivity* of OTFS system with an ideal or rectangular prototype window function (PWF) [9], [10]. These features provide the basis for signal detection and waveform design of OTFS system as well as Radar research.

OTFS initially uses the ideal PWF for perfect reconstruction (PR). However, it is not available in practice [1]. Subsequently, the OTFS system with rectangular PWFs was introduced in [9]. With appropriate signal detection methods, the system can achieve the same bit error rate (BER) as an OTFS system using ideal PWFs, but the resulting out-of-band emission (OOBE) is too high. For reducing the OOBE, the OTFS system uses a prolate spheroidal function with good localization in both time and frequency domain to replace the rectangular PWF [10]. It is worth considering that the function is of high computational complexity and insufficient flexibility. General frequency division multiplexing (GFDM) can share the system architecture with OTFS by signal permutation [11]. This provides the possibility of combining GFDM with OTFS. Unfortunately, GFDM is sensitive to noise interference when applying zero-forcing equalization for perfect signal reconstruction [12]. As a variant of GFDM, bi-orthogonal frequency division multiplexing (BFDM) allows the arbitrary design of PWFs with bi-orthogonal properties, thus avoiding the sensitivity of the inverse matrix to noise errors [13], [14]. Furthermore, BFDM can provide lower OOBE and more design freedom than OFDM, which are conducive to big data transmission and multi-user scenarios [15]. Inspired by the above, we propose a scheme using BFDM modulation in the OTFS system, where the bi-orthogonal property of PWFs can satisfy the PR condition.

Different signal detection approaches are currently explored for decoding and interference mitigation in OTFS systems [16]–[19]. In [16], soft symbol feedback is attached to the minimum mean square error (MMSE) equalizer to improve BER performance further because a single MMSE equalizer cannot help OTFS signals achieve full diversity. Li et al. [17] first used a single-tap equalizer in the frequency domain to eliminate multipath interference, then designed

Manuscript received April 12, 2021.
Manuscript revised July 23, 2021.
Manuscript publicized August 27, 2021.

[†]The authors are with the College of Artificial Intelligence, Beijing University of Posts and Telecommunications, Beijing, 100876, China.
[††]The author is with the Graduate School of Informatics and Engineering, The University of Electro-Communications, Tokyo, 182-8585 Japan.
a) E-mail: wutingyao@bupt.edu.cn
b) E-mail: zhisonbie@bupt.edu.cn (Corresponding author)
c) E-mail: celimuge@uec.ac.jp
DOI: 10.1587/transfun.2021EAP1030

*The input-output relation of the OTFS-BFDM system can be represented by an equivalent channel matrix which is proved to be sparsely-connected in Sect. 4. Therefore, the term "sparsely-connected system" can be used in some instances for convenience.

a DD-domain equalizer to alleviate the residual interference caused by Doppler spread. All the above methods are based on MMSE equalization, the former has high computational complexity, while the latter fails to obtain full diversity. Then Thaj and Viterbo proposed an iterative signal detection method with maximal ratio combining [18]. Some null symbols are placed in the DD-domain lattice to use the block-circulant property of the channel matrix. Thus the spectral efficiency is reduced to some extent. In [19], a signal detection method based on message passing (MP) algorithm was proposed, which follows the joint maximum posterior probability criterion for symbol-to-symbol detection and can simultaneously implement equalization and decoding. Moreover, the MP detector can be coupled with the DD channel to obtain full diversity without spectrum loss. Analysis results show that the MP detector has lower linear complexity and near-optimal performance. As mentioned in [20], MP detection enables the MIMO-OTFS system to obtain excellent BER performance under the Doppler shift of 1880 Hz. Therefore, the MP algorithm can be considered for signal detection and decoding for the OTFS-BFDM system.

The key premise of MP algorithms with low complexity is the sparsity of system because the symbol information is transmitted and iterated based on a sparse factor graph during signal detection. [21] shows a GFDM system with indexed modulation. Since the symbol information is only transmitted on the activated sub-carrier, a sparse matrix can be formed by the product of the GFDM modulation matrix and the channel matrix. On this sparse matrix, MP detection can be carried out. Raviteja et al. [9] derived the structure between the input and output of OTFS system is sparsely-connected so that MP decoding can be used. To sum up, before the OTFS-BFDM system performs MP decoding, it is necessary to verify the sparse-connectivity of the system.

OTFS can obtain the same low peak-to-average ratio (PAPR) as a single carrier frequency division multiple access (SC-FDMA) in small data frames [22]. However, as the number of symbols per frame increases, the PAPR becomes unbearably high [23]. In Sect. 4, we verify the PAPR performance of OTFS-BFDM signals through simulation. The results show that OTFS-BFDM signals also have the above PAPR features and can achieve the same PAPR as OTFS signals by optimizing PWFs. The key contributions of this paper can be summarized as follows:

1. The input-output relation of the OTFS-BFDM system is described in matrix form;
2. We deduce that the OTFS-BFDM system is sparsely-connected by analyzing the equivalent channel matrix. Therefore, the low complexity MP decoding algorithm can be adopted at the receiver.
3. The performances of power spectral density (PSD), PAPR, and BER of OTFS-BFDM system with different PWFs are compared.

The remainder of the paper is organized as follows. Section 2 gives a system-level description of OTFS-BFDM system in matrix forms. Section 3 elaborates the derivation of the sparse-connectivity of OTFS-BFDM system. In Sect. 4, the PSD and PAPR of the OTFS-BFDM system with different PWFs are compared through simulation. Section 5 analyzes the simulation results for BER performance comparison. Finally, Sect. 6 presents our research conclusions.

2. OTFS-BFDM System Model

This section gives a system-level description of OTFS-BFDM in matrix forms. We first review the OTFS transform and the polyphase implementation of BFDM, then elaborate on the input-output relationship of OTFS-BFDM system.

Figure 1 indicates the OTFS-BFDM system model. We assume that the transmission frame has a duration of NT and a bandwidth of $M\Delta f$, where $\Delta f = 1/T$ is the sub-carrier spacing. Let $D[m,n]$ be the n-th sub-symbol on the m-th sub-carrier in the TF domain. Correspondingly, the DD domain signals are quasi-period with a delay period $\tau = 1/\Delta f$ and a Doppler period $v = 1/T$. The 2D symbol $d[l,k]$ (e.g., 4QAM symbol) is distributed on the $(l/M\Delta f, k/NT)$ lattice point in the DD domain. At the transmitter, $d[l,k]$ is first mapped to the TF domain sampling $D[m,n]$ by ISFFT transform, where each $d[l,k]$ modulates a 2D basis function that completely spans the duration and bandwidth of the TF domain. Then $D[m,n]$ is modulated into the time-domain signal $\tilde{s}(\ell)$ transmitted on the wireless channel by a BFDM modulator, where each sub-carrier is pulse shaped by a circularly shifted PWF. At the receiver, the wireless signal $\tilde{s}(\ell)$ is first demodulated to the TF domain through the BFDM demodulator and then mapped to the DD domain using the SFFT transform. It can be seen that the OTFS-BFDM system performs ISFFT and SFFT transform on the BFDM system.

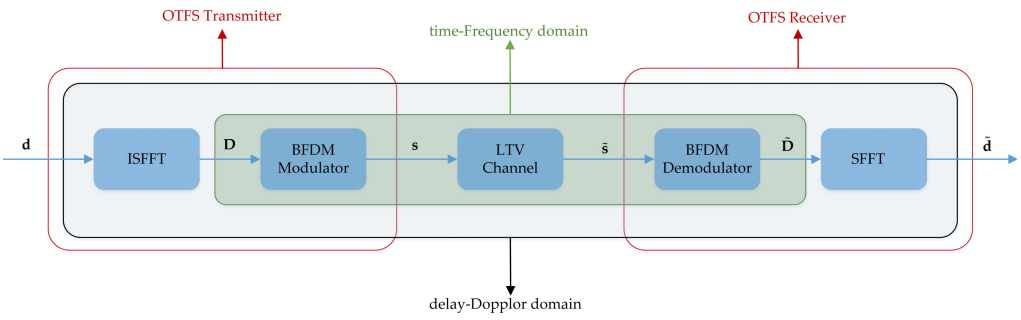

Fig. 1 OTFS-BFDM system model.

2.1 ISFFT Transform and BFDM Modulation

ISFFT and SFFT are essentially domain transformations of matrices. On the DD plane, the $MN \times 1$ symbol vector on each transmission frame can be represented by

$$\mathbf{d} = [\mathbf{d}_0^T, \mathbf{d}_1^T, \cdots, \mathbf{d}_{N-1}^T]^T, \tag{1}$$

where $\mathbf{d}_i = [d[0,i], d[1,i], \cdots, d[M-1,i]]^T, 0 \le i \le N-1$.

After $\mathbf{d}$ is pre-processed by ISFFT transform, the TF domain signal $\mathbf{D}$ is generated as

$$\mathbf{D} = (\mathbf{F}_N^{-1} \otimes \mathbf{F}_M)\mathbf{d}. \tag{2}$$

In (2), $\otimes$ denotes the Kronecker product, $\mathbf{F}_n^{-1}$ and $\mathbf{F}_n$ are the normalized n-point IDFT and DFT matrices, respectively.

We know that the BFDM system is based on the cyclic convolutional filter bank (CCFB) structure. According to the polyphase implementation principle of the M-channel CCFB, the modulation matrix of BFDM can be expressed as

$$\mathbf{A} = \underbrace{\begin{bmatrix} \mathbf{P}_0 & \mathbf{P}_{N-1} & \cdots & \mathbf{P}_1 \\ \mathbf{P}_1 & \mathbf{P}_0 & \cdots & \mathbf{P}_2 \\ \vdots & \vdots & \ddots & \vdots \\ \mathbf{P}_{N-1} & \mathbf{P}_{N-2} & \cdots & \mathbf{P}_0 \end{bmatrix}}_{\mathbf{P}} \begin{bmatrix} \mathbf{F}_M^{-1} & & & \\ & \ddots & & \\ & & \mathbf{F}_M^{-1} & \\ & & & \mathbf{F}_M^{-1} \end{bmatrix}. \tag{3}$$

Suppose $p(\ell)$ is the PWF of the BFDM analysis filter bank with length $L = MN$. In (3), $\mathbf{P}$ is an $L \times L$ block-circulant analysis filter coefficient matrix of the BFDM system. The matrix element $\mathbf{P}_i$ consisting of $p(\ell)$ is written as

$$\mathbf{P}_i = \begin{bmatrix} P(iM) & & & \\ & P(iM+1) & & \\ & & \ddots & \\ & & & P(iM+M-1) \end{bmatrix}, \tag{4}$$

where $0 \le i \le N-1$.

When $\mathbf{D}$ passes through the BFDM modulator, it will be converted into the time-domain signal $\mathbf{s}$ transmitted on the wireless channel as

$$\begin{aligned} \mathbf{s} &= \mathbf{A} \cdot \mathbf{D} \\ &= \mathbf{P}(\mathbf{I}_N \otimes \mathbf{F}_M^{-1})(\mathbf{F}_N^{-1} \otimes \mathbf{F}_M)\mathbf{d} \\ &= \mathbf{P}(\mathbf{F}_N^{-1} \otimes \mathbf{I}_M)\mathbf{d}, \end{aligned} \tag{5}$$

where $\mathbf{I}_M$ denotes an $M \times M$ identity matrix.

2.2 SFFT Transform and BFDM Demodulation

The condition for perfect signal reconstruction of BFDM is

$$\mathbf{AB} = \mathbf{I}, \tag{6}$$

where $\mathbf{A}$ and $\mathbf{B}$ are the full-rank modulation and demodulation matrices of the BFDM system respectively, and $\mathbf{I}$ is an $L \times L$ identity matrix.

Once $\mathbf{P}$ is determined, we can get the synthesis filter coefficient matrix $\mathbf{Q}$ by calculating $\mathbf{Q} = \mathbf{P}^{-1}$. The PWF $q(\ell)$ of synthesis filter bank can be extracted from the first-row matrix element of $\mathbf{Q}$. Therefore, BFDM allows the arbitrary design of $p(\ell)$ at the transmitter due to the PR condition. In this case, the PWF $p(\ell)$ and $q(\ell)$ are considered to be bi-orthogonal. Then the demodulation matrix $\mathbf{B}$ can be derived from (3) and (6) in this form

$$\mathbf{B} = \begin{bmatrix} \mathbf{F}_M & & & \\ & \ddots & & \\ & & \mathbf{F}_M & \\ & & & \mathbf{F}_M \end{bmatrix} \underbrace{\begin{bmatrix} \mathbf{Q}_0 & \mathbf{Q}_1 & \cdots & \mathbf{Q}_{N-1} \\ \mathbf{Q}_{N-1} & \mathbf{Q}_0 & \cdots & \mathbf{Q}_{N-2} \\ \vdots & \vdots & \ddots & \vdots \\ \mathbf{Q}_1 & \mathbf{Q}_2 & \cdots & \mathbf{Q}_0 \end{bmatrix}}_{\mathbf{Q}}, \tag{7}$$

with the matrix element

$$\mathbf{Q}_i = \begin{bmatrix} q(iM) & & & \\ & q(iM+1) & & \\ & & \ddots & \\ & & & q(iM+M-1) \end{bmatrix}, \tag{8}$$

$(0 \le i \le N-1)$.

At the receiving side of OTFS-BFDM, $\tilde{\mathbf{s}}$ is obtained after removing the CP. Through the BFDM demodulator and SFFT transform, $\tilde{\mathbf{s}}$ can be mapped as the signal $\tilde{\mathbf{d}}$ in the DD domain, as follows

$$\begin{aligned} \tilde{\mathbf{d}} &= (\mathbf{F}_N \otimes \mathbf{F}_M^{-1})\mathbf{B}\tilde{\mathbf{s}} \\ &= (\mathbf{F}_N \otimes \mathbf{F}_M^{-1})(\mathbf{I}_N \otimes \mathbf{F}_M)\mathbf{Q}\tilde{\mathbf{s}} \\ &= (\mathbf{F}_N \otimes \mathbf{I}_M)\mathbf{Q}\tilde{\mathbf{s}}. \end{aligned} \tag{9}$$

where $(\mathbf{F}_N \otimes \mathbf{F}_M^{-1})$ represents the SFFT transform.

3. Input-Output Relationship of OTFS-BFDM Systems

Assume that a linear time-varying (LTV) channel has P discrete propagation paths. The channel's impulse response in the DD domain can be expressed as

$$h(\tau, \upsilon) = \sum_{p=1}^{P} h_p \delta(\tau - \tau_p)\delta(\upsilon - \upsilon_p), \tag{10}$$

where h_p, τ_p and υ_p are the complex attenuation coefficient, delay and Doppler frequency respectively. As a result, the delay and Doppler-shift taps for p-th path can be given as $\tau_p = l_p/M\Delta f$ and $\upsilon_p = k_p/NT$.

In the OTFS-BFDM system, a CP with length P-1 is appended to the signal vector $\mathbf{s}$ before transmission. When the transmission signal reaches the receiver, the CP is removed. The received signal after removing the CP can be expressed as

$$\tilde{\mathbf{s}} = \mathbf{H}\mathbf{s} + \mathbf{w}. \tag{11}$$

In (11), $\mathbf{w}$ is a white Gaussian noise vector with the variance σ_w^2, and $\mathbf{H}$ is an $L \times L$ channel matrix, where

$$\mathbf{H} = \sum_{p=1}^{P} h_p \mathbf{\Pi}^{l_p} \mathbf{\Delta}^{k_p}, \tag{12}$$

with the circulant delay-shift matrix

$$\mathbf{\Pi} = circ\{[0, 1, 0, \cdots, 0]_{L\times 1}\} \tag{13}$$

and diagonal Doppler-shift matrix

$$\mathbf{\Delta} = diag\{1, e^{j2\pi/MN}, \cdots, e^{j2\pi(MN-1)/MN}\}. \tag{14}$$

Therefore, combining (5), (9) and (11), we can get the input and output relationship of OTFS-BFDM system as follows

$$\begin{aligned}\tilde{\mathbf{d}} &= (\mathbf{F}_N \otimes \mathbf{F}_M^{-1})\mathbf{B}\tilde{\mathbf{s}} \\ &= (\mathbf{F}_N \otimes \mathbf{F}_M^{-1})(\mathbf{I}_N \otimes \mathbf{F}_M)\mathbf{Q}\mathbf{H}\mathbf{P}(\mathbf{F}_N^{-1} \otimes \mathbf{I}_M)\mathbf{d} \\ &+ (\mathbf{F}_N \otimes \mathbf{F}_M^{-1})(\mathbf{I}_N \otimes \mathbf{F}_M)\mathbf{Q}\mathbf{w} \\ &= \underbrace{(\mathbf{F}_N \otimes \mathbf{I}_M)\mathbf{Q}\mathbf{H}\mathbf{P}(\mathbf{F}_N^{-1} \otimes \mathbf{I}_M)}_{\mathbf{H}_{eq}}\mathbf{d} + \underbrace{(\mathbf{F}_N \otimes \mathbf{I}_M)\mathbf{Q}\mathbf{w}}_{\tilde{\mathbf{w}}},\end{aligned} \tag{15}$$

where $\mathbf{H}_{eq} = (\mathbf{F}_N \otimes \mathbf{I}_M)\mathbf{Q}\mathbf{H}\mathbf{P}(\mathbf{F}_N^{-1} \otimes \mathbf{I}_M)$ is the equivalent channel matrix, and $\tilde{\mathbf{w}}$ represents the channel noise vector. If $\mathbf{P}$ and $\mathbf{Q}$ are identity matrices, the simplified (15) can be simplified as follows

$$\tilde{\mathbf{d}} = (\mathbf{F}_N \otimes \mathbf{I}_M)\mathbf{H}(\mathbf{F}_N^{-1} \otimes \mathbf{I}_M)\mathbf{d} + (\mathbf{F}_N \otimes \mathbf{I}_M)\mathbf{w}, \tag{16}$$

representing the input-output relationship of the OTFS system.

4. Sparse-Connectivity Analysis of OTFS-BFDM Systems

To use MP decoding in the OTFS-BFDM system, we further derive the sparse-connectivity of the equivalent channel matrix. From (3) and (4), the block-circulant property of the matrix $\mathbf{P}$ leads to

$$\mathbf{P} = (\mathbf{F}_N^{-1} \otimes \mathbf{I}_M)\mathbf{\Lambda}(\mathbf{F}_N \otimes \mathbf{I}_M), \tag{17}$$

where $\mathbf{\Lambda} = diag(\mathbf{\Lambda}_0, \mathbf{\Lambda}_1, \cdots, \mathbf{\Lambda}_{N-1})$, $\mathbf{\Lambda}_n \in \mathbb{C}^{M\times M}$ can be calculated by

$$\begin{aligned}&\mathbf{\Phi}(i,j) = [\mathbf{P}_0(i,j), \mathbf{P}_1(i,j), \cdots, \mathbf{P}_{N-1}(i,j)]^T, \\ &0 \le i, j \le M-1.\end{aligned} \tag{18}$$

and

$$\begin{aligned}&[\mathbf{\Lambda}_0(i,j), \mathbf{\Lambda}_1(i,j), \cdots, \mathbf{\Lambda}_{N-1}(i,j)] = \sqrt{N}\mathbf{F}_N\mathbf{\Phi}(i,j), \\ &0 \le i, j \le M-1.\end{aligned} \tag{19}$$

From (4) and (18), we get that $\mathbf{\Phi}(i,j)$ is an N-dimensional vector composed of $\mathbf{P}_n(i,j)$. Moreover, all elements in $\mathbf{\Phi}(i,j)$ are zero when $i = j$ because $\mathbf{P}_n$ is a diagonal matrix. For each sub-matrix $\mathbf{\Lambda}_n$, only the elements on its principal diagonal can be calculated by the Fourier transform of $\mathbf{\Phi}(i,j)$ described in (17). Consequentially, $\mathbf{\Lambda}$ is also a diagonal matrix according to $\mathbf{\Lambda} = diag(\mathbf{\Lambda}_0, \mathbf{\Lambda}_1, \cdots, \mathbf{\Lambda}_{N-1})$.

By (6), (7) and (17), the synthesis filter coefficient matrix $\mathbf{Q}$ can be reinterpreted as

$$\mathbf{Q} = (\mathbf{F}_N^{-1} \otimes \mathbf{I}_M)\mathbf{\Lambda}^{-1}(\mathbf{F}_N \otimes \mathbf{I}_M), \tag{20}$$

where $\mathbf{\Lambda}^{-1}$ is the inverse of Λ, both $\mathbf{\Lambda}^{-1}$ and $\mathbf{\Lambda}$ are diagonal matrices.

By (15), (17) and (20), we re-express the input and output relationship of OTFS-BFDM system as follow

$$\begin{aligned}\tilde{\mathbf{d}} &= (\mathbf{F}_N \otimes \mathbf{I}_M)(\mathbf{F}_N^{-1} \otimes \mathbf{I}_M)\mathbf{\Lambda}^{-1}(\mathbf{F}_N \otimes \mathbf{I}_M)\mathbf{H} \\ &\cdot (\mathbf{F}_N^{-1} \otimes \mathbf{I}_M)\mathbf{\Lambda}(\mathbf{F}_N \otimes \mathbf{I}_M)(\mathbf{F}_N^{-1} \otimes \mathbf{I}_M)\mathbf{d} \\ &+ (\mathbf{F}_N \otimes \mathbf{I}_M)(\mathbf{F}_N^{-1} \otimes \mathbf{I}_M)\mathbf{\Lambda}^{-1}(\mathbf{F}_N \otimes \mathbf{I}_M)\mathbf{w} \\ &= \underbrace{\mathbf{\Lambda}^{-1}(\mathbf{F}_N \otimes \mathbf{I}_M)\mathbf{H}(\mathbf{F}_N^{-1} \otimes \mathbf{I}_M)\mathbf{\Lambda}}_{\mathbf{H}_{eq}}\mathbf{d} + \underbrace{\mathbf{\Lambda}^{-1}(\mathbf{F}_N \otimes \mathbf{I}_M)\mathbf{w}}_{\tilde{\mathbf{w}}},\end{aligned} \tag{21}$$

In (16), the equivalent channel matrix of the OTFS system using rectangular PWFs is given as

$$\mathbf{H}_{eq}^{Rec} = (\mathbf{F}_N \otimes \mathbf{I}_M)\mathbf{H}(\mathbf{F}_N^{-1} \otimes \mathbf{I}_M). \tag{22}$$

Raviteja et al. [10] concluded that $\mathbf{H}_{eq}^{Rec}$ is sparse, and the factor graph modeled by $\mathbf{H}_{eq}^{Rec}$ is sparsely-connected. As explained in [19], variable nodes and observation nodes pass information to each other through the factor graph in MP signal detection. Thus each variable node can be connected with only a few observation nodes, which greatly reduces the computational complexity of the MP algorithm.

Combining (21) and (22), we get the equivalent channel matrix of OTFS-BFDM system as

$$\mathbf{H}_{eq} = \mathbf{\Lambda}^{-1}\mathbf{H}_{eq}^{\mathrm{Re}\,c}\mathbf{\Lambda}, \tag{23}$$

where $\mathbf{H}_{eq}$is obtained by multiplying different diagonal matrices on the left and right sides of the matrix $\mathbf{H}_{eq}^{Rec}$. Since the diagonal matrix $\mathbf{\Lambda}^{-1}$ and $\mathbf{\Lambda}$ does not affect the sparsity of the matrix, $\mathbf{H}_{eq}$ is also sparse. Referring to the factor graph model in [9], we conclude that the OTFS-BFDM system is also sparsely-connected.

5. OOBE and PAPR Performance of OTFS-BFDM Systems

The OTFS-BFDM system can be called a circularly pulse shaped OTFS system, which allows the arbitrary design of bi-orthogonal PWFs with good frequency-domain localization, such as root raised cosine (RRC) function and raised cosine (RC) function. This section compares the PSD and

PAPR performance of the OTFS-BFDM system with different PWFs through simulation. The results show that i) OTFS-BFDM systems using RRC or RC PWFs can provide lower OOBE than conventional OTFS systems; ii) OTFS-BFDM systems have relatively low PAPR under small packets, but with the increase of Doppler bins and roll-off factor, PAPR becomes unbearably high.

5.1 OOBE

The conventional OTFS system adopts a rectangular PWF with a sine function spectrum shape. Side lobes of each subcarrier have slower oscillation attenuation, which causes high OOBE in the entire power spectrum and interferes with adjacent channel signals. In order to suppress the OOBE, we use BFDM modulation in the OTFS system. The OOBE of OTFS-BFDM mainly depends on the PSD of the BFDM modulation block. The PSD of the baseband signal can be calculated as

$$PSD(f) = \lim_{T\to\infty}\left(\frac{1}{T}E\left\{\left|\int_{-T/2}^{T/2} s(t)e^{-j2\pi ft}dt\right|^2\right\}\right), \quad (24)$$

where $E\{\cdot\}$ denotes mathematical expectation, $s(t)$ is obtained by passing $s(\ell)$ through a digital-to-analog converter, and T is a transmit block interval. Assuming that the data symbols are independent and identically distributed, the PSD of the BFDM system can be expressed as [24]

$$PSD(f) = \frac{1}{NT_0}\sum_{m,n}|P_n(f-\frac{m}{T_0})|^2. \quad (25)$$

In (25), $P_n(f)$ is the DFT of $p[0,n]_\ell$ and T_0 is the symbol duration, $p[m,n]_\ell$represents the time-domain impulse response of the PWF $p(\ell)$ with the cyclic time shift and frequency shift, can be expressed as

$$p[m,n]_\ell = p[<(\ell-nm)>_L]e^{-j2\pi\frac{m}{M}\ell} \quad (26)$$

when $p(\ell)$ is a rectangular function with the length M, the BFDM block can also be regarded as a cyclic convolution block based on OFDM modulation. The OOBE of the BFDM system can be defined as the ratio of the total energy in the ***OOB*** frequency range to the total energy in the passband ***B***:

$$OOBE = \frac{\boldsymbol{B}}{\boldsymbol{OOB}}\cdot\frac{\int\limits_{f\in OOB} PSD(f)df}{\int\limits_{f\in B} PSD(f)df}. \quad (27)$$

Based on the Barren-Law theorem [25], we know that it is impossible to obtain a modulation scheme with well-localized PWFs in both time and frequency while main-taining orthogonality and Nyquist rate. Figure 2(a) shows the time-domain response of PWFs with different roll-off factors when $N = 31$, $M = 32$. The simulation results show that the tail attenuation of rectangular PWFs is the slowest in time domain. The smaller the roll-off factor of RRC and RC PWFs, the slower the tail attenuation of PWF, and the better the frequency-domain localization of PWF. In addition, under the same roll-off factor, the time-domain localization effect of RC is slightly better than that of RRC.

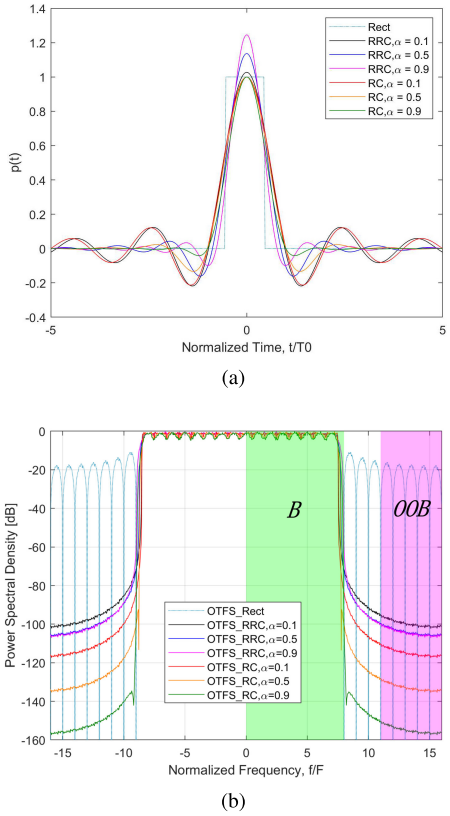

Fig. 2 (a) describes the time-domain response of PWFs with different roll-off factors when $N = 31$, $M = 32$; (b) describes the PSD of OTFS-BFDM using different PWFs when the number of activated sub-carriers is 16. ***B*** and ***OOB*** are used to distinguish the in-band and out-of-band regions, and a guard bandwidth is considered between the two regions. α is the roll-off factor of PWF.

Figure 2(b) illustrates the PSD of OTFS-BFDM system with different PWFs when the number of activated subcarriers is 16. We can evaluate the OOBE performance of the system by the out-of-band PSD emission form (27). As shown in Fig. 2(b), when the OTFS-BFDM system uses the RRC PWF with a roll-off factor of 0.1, the PSD can be reduced by 84 dB compared with the OTFS-BFDM system using rectangular PWFs. Moreover, the larger the roll-off factor of PWF, the lower the OOBE of system. Overall, the OOBE of OTFS-BFDM system using RRC or RC PWFs is much better than that of the OTFS-BFDM system using rectangular PWFs.

Therefore, non-rectangular PWFs with better frequency-domain localization can significantly reduce the OOBE of OTFS-BFDM system. This feature is of great significance in 5G multi-user scenarios.

5.2 PAPR

The PAPR of the discrete-time samples of the OTFS-BFDM

signal $s(\ell)$ on each frame is defined as [26]

$$PAPR = 10\log \frac{\max\limits_{0\le \ell \le O\cdot(L-1)} \{|s(\ell)|^2\}}{E\{|s(\ell)|^2\}}, \tag{28}$$

where O is the oversampling factor assumed to be 4.

In practice, the complementary cumulative distribution function (CCDF) is used to evaluate the PAPR performance of system by calculating the probability that the PAPR of each sample value exceeds the predefined threshold $PAPR_0$. The CCDF has statis-tical properties, which can be expressed as

$$\begin{aligned} C_{PAPR}(PAPR_0) &= \Pr(PAPR > PAPR_0) \\ &= 1 - \Pr(PAPR \le PAPR_0) \\ &= 1 - (1 - \exp(-PAPR_0))^{OL}. \end{aligned} \tag{29}$$

In the OTFS-BFDM system, M sub-carrier signals of the transmitter are superimposed on each other. If the sub-carrier phases are consistent at a specific moment, a high peak power will be generated. We can grasp the PAPR performance of OTFS-BFDM system more intuitively through simulation. Figure 3(a) depicts the CCDF of PAPR of the OTFS-BFDM system with 4-QAM symbol mapping under different N values when $M = 32$ and $\alpha = 0.1$. Under different PWFs, the CCDF curves of PAPR of OTFS-BFDM system are almost consistent because these PWFs in the time domain have close peaks. With the increase of N, the CCDF of PAPR of OTFS-BFDM system will eventually exceed that of OFDM system. When $N = 4$, the $PAPR_0$ of OTFS-BFDM system with RRC PWF is 1 dB lower than that of OFDM system at the CCDF of 10^{-3}. However, when N increases to 64, the $PAPR_0$ of OTFS-BFDM system with RRC PWFs is 0.5 dB higher than that of OFDM system at the CCDF of 10^{-3}. As can be seen from Fig. 3(a), the PAPR becomes unbearably high with increasing N in the OTFS-BFDM system.

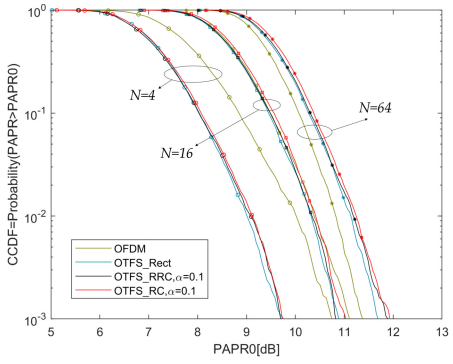

(a)

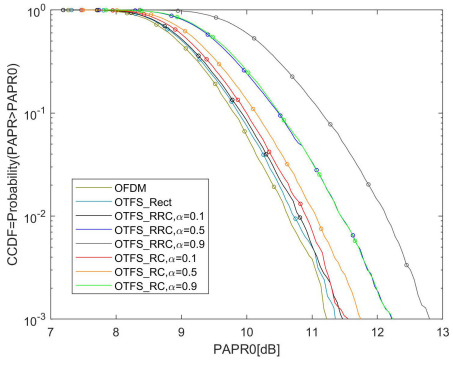

(b)

Fig. 3 (a) describes the CCDF of PAPR of OTFS-BFDM systems with different N values ($M = 32$, 4-QAM); (b) describes the CCDF of PAPR of OTFS-BFDM systems with different PWFs ($M = 32$, $N = 31$, 4-QAM).

Figure 3(b) reveals that the CCDF of PAPR of OTFS-BFDM system with different PWFs when $M = 32$, $N = 31$. As shown in Fig. 3(b), the $PAPR_0$ of OTFS-BFDM system with different PWFs is greater than that of OFDM system at any given CCDF, which confirms that the PAPR performance of OTFS-BFDM system deteriorates in the case of large packets. Under the same roll-off factor, because the peak value of RC PWF is smaller than that of RRC PWF, the PAPR of OTFS-BFDM system using RC PWFs is lower than that of OTFS-BFDM system using RRC PWFs. Also, the smaller the roll-off factor of PWF, the better the PAPR of OTFS-BFDM system. Figure 3(a) can explain the above that the peak value becomes less sharp as the roll-off factor decreases for the same PWF.

Therefore, by optimizing the PWF, OTFS-BFDM can achieve nearly the same PAPR as OTFS while having a lower OOBE than OTFS.

6. BER Simulation

In this section, we evaluate the BER performance of OTFS-BFDM system through numerical simulation. The delay-Doppler profile considered is shown in Table 1, including three different maximum Doppler shifts with the path index of 5. Other relevant simulation parameters are summarized in Table 2.

Figure4 depicts the BER performance of OTFS-BFDM systems on the delay-Doppler channels. Figure 4(a), 4(b) and 4(c) respectively correspond to the channel scenes with

Table 1 Delay-Doppler profile for the channel model with path = 5.

Path index	1	2	3	4	5
Delay (μs)	0	2.08	4.17	6.25	8.33
Doppler1 (Hz)	0	0	0	483.87	967.74
Doppler2 (Hz)	0	0	483.87	967.74	1451.61
Doppler3 (Hz)	0	483.87	967.74	1451.61	1935.48

Table 2 Simulation parameters.

Parameter	Value
Carrier frequency (GHz)	4
Subcarrier spacing (kHz)	15
Frame size (M, N)	(32,31)
Modulation scheme	4-QAM
CP (μs)	10.42
Channel estimation	ideal

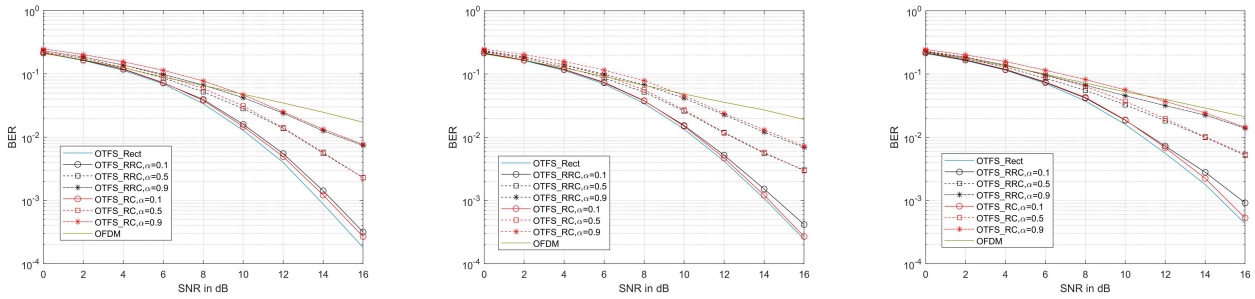

(a) (b) (c)

Fig. 4 BER performance of OTFS-BFDM systems on the delay-Doppler channel with different maximum Doppler shift. (a) maximum Doppler shift of 967.74 Hz; (b) maximum Doppler shift of 1451.61 Hz; (c) maximum Doppler shift of 1935.48 Hz.

maximum Doppler shifts of 967.74 Hz, 1451.61 Hz and 1935.48 Hz. We use MP decoding for all the systems in the experiment since the OFDM system is proved to be sparse by [9]. As shown in Fig. 4(a), the BER of OTFS-BFDM system is much lower than that of OFDM system and with the increase of signal-to-noise ratio (SNR), BER gap becomes more and more serious. Besides, the slower the time-domain attenuation of PWFs, the lower the inter-carrier interference. Therefore, the BER of an OTFS-BFDM system also decreases as the PWF roll-off factor becomes smaller. When the RC PWF with $\alpha = 0.1$ is adopted, the BER of OTFS-BFDM system is close to that of OTFS system. However, with the increase of α value, the BER difference between OTFS-BFDM system using RRC or RC PWF and OTFS system is accelerated.

Also, the BER performance of OTFS-BFDM system decreases with the increase of Doppler shift. When the OTFS-BFDM system uses the RRC PWF of $\alpha = 0.1$ to simulate on channels with maximum Doppler shift of 967.74 Hz, 1451.61 Hz and 1935.48 Hz, the BERs obtained are 3.178×10^{-4}, 4.201×10^{-4} and 9.191×10^{-3}, respectively. Meanwhile, Fig. 4(b) and Figure 4(c) show similar BER performance to Fig. 4(a).

In general, the BER of OTFS- BFDM with non-rectangular PWFs is better than OFDM but worse than OTFS on high Doppler channels. The PWF with better frequency domain localization can reduce the inter carrier interference and BER.

7. Conclusions

In this paper, we derives the equivalent channel matrix of OTFS-BFDM system and proves that the structure between the input and output of the system is sparsely-connected. Furthermore, the PAPR, PSD and BER of OTFS-BFDM system with different PWFs are compared by simulation. OTFS-BFDM with longer non-rectangular PWFs can achieve lower OOB power leakage and more flexible design freedom compared with OTFS. In particular, by adopting the appropriate PWF, OTFS-BFDM can approach the PAPR and BER performance of OTFS while reducing OOBE. Therefore, the research on OTFS-BFDM in this paper is of positive significance for IoT and multi-user scenarios in 5G high-speed motion.

References

[1] R. Hadani, S. Rakib, M. Tsatsanis, A. Monk, A.J. Goldsmith, A.F. Molisch, and R. Calderbank, "Orthogonal time frequency space modulation," 2017 IEEE Wireless Communications and Networking Conference (WCNC), pp.1–6, 2017.

[2] R. Hadani, S. Rakib, S. Kons, M. Tsatsanis, A. Monk, C. Ibars, J. Delfeld, Y. Hebron, A.J. Goldsmith, A.F. Molisch, and A.R. Calderbank, "Orthogonal time frequency space modulation," CoRR, vol.abs/1808.00519, 2018. http://arxiv.org/abs/1808.00519

[3] R. Hadani and A. Monk, "OTFS: A new generation of modulation addressing the challenges of 5G," CoRR, vol.abs/1802.02623, 2018. http://arxiv.org/abs/1802.02623

[4] A. Farhang, A. RezazadehReyhani, L.E. Doyle, and B. Farhang-Boroujeny, "Low complexity modem structure for OFDM-based orthogonal time frequency space modulation," IEEE Wireless Commun. Lett., vol.7, no.3, pp.344–347, 2018.

[5] R. Hadani, S. Rakib, A.F. Molisch, C. Ibars, A. Monk, M. Tsatsanis, J. Delfeld, A. Goldsmith, and R. Calderbank, "Orthogonal time frequency space (OTFS) modulation for millimeter-wave communications systems," 2017 IEEE MTT-S International Microwave Symposium (IMS), pp.681–683, 2017.

[6] P. Raviteja, K.T. Phan, Y. Hong, and E. Viterbo, "Orthogonal time frequency space (OTFS) modulation based radar system," 2019 IEEE Radar Conference (RadarConf), pp.1–6, 2019.

[7] L. Gaudio, M. Kobayashi, B. Bissinger, and G. Caire, "Performance analysis of joint radar and communication using OFDM and OTFS," 2019 IEEE International Conference on Communications Workshops (ICC Workshops), pp.1–6, 2019.

[8] G.D. Surabhi, R.M. Augustine, and A. Chockalingam, "On the diversity of uncoded OTFS modulation in doubly-dispersive channels," IEEE Trans. Wireless Commun., vol.18, no.6, pp.3049–3063, 2019.

[9] P. Raviteja, K.T. Phan, Y. Hong, and E. Viterbo, "Interference cancellation and iterative detection for orthogonal time frequency space modulation," IEEE Trans. Wireless Commun., vol.17, no.10, pp.6501–6515, 2018.

[10] P. Raviteja, Y. Hong, E. Viterbo, and E. Biglieri, "Practical pulse-shaping waveforms for reduced-cyclic-prefix OTFS," IEEE Trans. Veh. Technol., vol.68, no.1, pp.957–961, 2019.

[11] A. Nimr, M. Chafii, M. Matthe, and G. Fettweis, "Extended GFDM framework: OTFS and GFDM comparison," 2018 IEEE Global Communications Conference (GLOBECOM), pp.1–6, 2018.

[12] M. Matthé, L.L. Mendes, and G. Fettweis, "Generalized frequency division multiplexing in a Gabor transform setting," IEEE Commun. Lett., vol.18, no.8, pp.1379–1382, 2014.

[13] H. Adouni, M. Hizem, and R. Bouallegue, "BFDM prototype for

cognitive radio systems," 10th International Conference on Wireless Communications, Networking and Mobile Computing (WiCOM 2014), pp.195–200, 2014.
[14] C. Huang, J. Wu, C. Wang, S. Hu, and G. Wu, "Waveform optimization of BFDM for massive connections support over dispersive channels," 2016 IEEE International Conference on Communication Systems (ICCS), pp.1–6, 2016.
[15] C. Zhang, K. Ota, J. Jia, and M. Dong, "Breaking the blockage for big data transmission: Gigabit road communication in autonomous vehicles," IEEE Commun. Mag., vol.56, no.6, pp.152–157, 2018.
[16] T. Zemen, M. Hofer, and D. Loeschenbrand, "Low-complexity equalization for orthogonal time and frequency signaling (OTFS)," CoRR, vol.abs/1710.09916, 2017. http://arxiv.org/abs/1710.09916
[17] L. Li, H. Wei, Y. Huang, Y. Yao, W. Ling, G. Chen, P. Li, and Y. Cai, "A simple two-stage equalizer with simplified orthogonal time frequency space modulation over rapidly time-varying channels," CoRR, vol.abs/1709.02505, 2017. http://arxiv.org/abs/1709.02505
[18] T. Thaj and E. Viterbo, "Low complexity iterative rake detector for orthogonal time frequency space modulation," 2020. https://arxiv.org/abs/2001.10703
[19] P. Raviteja, K.T. Phan, Q. Jin, Y. Hong, and E. Viterbo, "Low-complexity iterative detection for orthogonal time frequency space modulation," 2018 IEEE Wireless Communications and Networking Conference (WCNC), pp.1–6, 2018.
[20] M. Kollengode Ramachandran and A. Chockalingam, "MIMO-OTFS in high-Doppler fading channels: Signal detection and channel estimation," 2018 IEEE Global Communications Conference (GLOBECOM), pp.206–212, 2018.
[21] Y. Niu and J. Zheng, "Message passing algorithm for GFDM-IM detection," 2018 IEEE 23rd International Conference on Digital Signal Processing (DSP), pp.1–5, 2018.
[22] R1-1610446, "OTFS PAPR analysis," Discussion 8.1.1.1 3GPP TSG RA WG1 Meeting, Cohere Technologies, 2016. https://www.3gpp.org/ftp/TSG_RAN/WG1_RL1/TSGR1_86b/Docs/R1-1610446.zip
[23] G.D. Surabhi, R.M. Augustine, and A. Chockalingam, "Peak-to-average power ratio of OTFS modulation," IEEE Commun. Lett., vol.23, no.6, pp.999–1002, 2019.
[24] N. Michailow, M. Matthé, I.S. Gaspar, A.N. Caldevilla, L.L. Mendes, A. Festag, and G. Fettweis, "Generalized frequency division multiplexing for 5th generation cellular networks," IEEE Trans. Commun., vol.62, no.9, pp.3045–3061, 2014.
[25] M. Schellmann, Z. Zhao, H. Lin, P. Siohan, N. Rajatheva, V. Luecken, and A. Ishaque, "FBMC-based air interface for 5G mobile: Challenges and proposed solutions," 2014 9th International Conference on Cognitive Radio Oriented Wireless Networks and Communications (CROWNCOM), pp.102–107, 2014.
[26] A.S. Rajasekaran, M. Vameghestahbanati, M. Farsi, H. Yanikomeroglu, and H. Saeedi, "Resource allocation-based PAPR analysis in uplink SCMA-OFDM systems," IEEE Access, vol.7, pp.162803–162817, 2019.

Tingyao Wu received the B.Sc. and M.Sc. degrees in communication and information system from Guilin University Of Electronic Technology, china in 2007, and 2012, respectively. He is currently pursuing the Ph.D. degree in the College of Articial Intelligence, Beijing University of Posts and Telecommunications, Beijing, China. His current research interests include non-orthogonal multiple access and orthogonal time frequency space.

Zhisong Bie received his Ph.D. degree from Beijing University of Posts and Telecommunications, China in 2007. He is currently an associate professor with the School of Artificial Intelligence, Beijing University of Posts and Telecommnunications. His current research interests include wireless communication, AI, and mobile edge computing.

Celimuge Wu received his Ph.D. degree from The University of Electro-Communications, Japan in 2010. He is currently an associate professor with the Graduate School of Informatics and Engineering, The University of Electro-Communications. His current research interests include IoT, big data, AI, and mobile edge computing. He serves as an associate editor of IEEE Transactions on Network Science and Engineering, IEEE Transactions on Green Communications and Networking, China Communications, IEEE Access, Wireless Networks, IEICE Transactions on Communications, International Journal of Distributed Sensor Networks, and MDPI Sensors. He has been a guest editor of IEEE Transaction on Intelligent Transportation Systems, IEEE Transactions on Emerging Topics in Computational Intelligence, IEEE Computational Intelligence Magazine, ACM/Springer MONET etc. He is the chair of IEEE TCBD SIG on Big Data with Computational Intelligence and IEEE TCGCC SIG on Green Internet of Vehicles. He received IEEE Computer Society 2019 Best Paper Award Runner-Up. He is a senior member of IEEE.